Intracellular and Computational Characterization of the Intracortical Inhibitory Control of Synchronized Thalamic Inputs In Vivo

DIEGO CONTRERAS, ALAIN DESTEXHE, AND MIRCEA STERIADE
Laboratoire de Neurophysiologie, Faculté de Médecine, Université Laval, Quebec G1K 7P4, Canada

Contreras, Diego, Alain Destexhe, and Mircea Steriade. Intracellular and computational characterization of the intracortical inhibitory control of synchronized thalamic inputs in vivo. *J. Neurophysiol.* 78: 335–350, 1997. We investigated the presence and role of local inhibitory cortical control over synchronized thalamic inputs during spindle oscillations (7–14 Hz) by combining intracellular recordings of pyramidal cells in barbiturate-anesthetized cats and computational models. The recordings showed that *1*) similar excitatory postsynaptic potential (EPSP)/inhibitory postsynaptic potential (IPSP) sequences occurred either during spindles or following thalamic stimulation; *2*) reversed IPSPs with chloride-filled pipettes transformed spindle-related EPSP/IPSP sequences into robust bursts with spike inactivation, resembling paroxysmal depolarizing shifts during seizures; and *3*) dual simultaneous impalements showed that inhibition associated with synchronized thalamic inputs is local. Computational models were based on reconstructed pyramidal cells constrained by recordings from the same cells. These models showed that the transformation of EPSP/IPSP sequences into fully developed spike bursts critically needs a relatively high density of inhibitory currents in the soma and proximal dendrites. In addition, models predict significant Ca^{2+} transients in dendrites due to synchronized thalamic inputs. We conclude that synchronized thalamic inputs are subject to strong inhibitory control within the cortex and propose that *1*) local impairment of inhibition contributes to the transformation of spindles into spike-wave-type discharges, and *2*) spindle-related inputs trigger Ca^{2+} events in cortical dendrites that may subserve plasticity phenomena during sleep.

INTRODUCTION

During sleep spindles, thalamocortical (TC) cells discharge high-frequency spike bursts that are transmitted to the cerebral cortex, thus generating rhythmic synaptic responses in cortical cells that underlie the spindle oscillation observable at the electroencephalographic (EEG) level (Contreras and Steriade 1996; Steriade et al. 1990). Spindle oscillations are sequences of depth-negative (surface-positive) EEG waves at 7–14 Hz, lasting 1–3 s and recurring every 2–5 s (Steriade and Deschênes 1984). The synchronized nature of thalamic inputs to dendrites of neocortical pyramidal cells contrasts with the relatively low rate of discharge of these cells during resting sleep accompanied by spindle oscillations (Evarts 1964; Steriade et al. 1974). As we explore in this paper, a possible explanation is that strong excitatory postsynaptic potentials (EPSPs) indeed occur in pyramidal cells' dendrites but remain invisible in somatic recordings because of the existence of strong feedforward inhibition. Such strong EPSPs are of high interest because they are likely to trigger Ca^{2+} entry in dendrites (Yuste and Tank 1996).

On the other hand, topical application of penicillin on cortex, which is supposed to produce a slight blockage of local GABAergic inhibition, generates paroxysmal depolarizing shifts (PDSs) in cortical cells in synchrony with EEG spikes of high amplitude, the so-called interictal spikes (Gloor et al. 1977; Matsumoto and Ajmone-Marsan 1964). The same procedure also gives rise to spike wave (SW) epileptiform discharges. Those results led to the hypothesis that, in the penicillin epilepsy model (Prince and Farrell 1963), SW results from a transformation of spindle-related thalamic inputs into ictal spikes, due to an increase in cortical excitability (Gloor et al. 1979, 1990). One prediction from the penicillin studies would be that during spindles, thalamic inputs are submitted to a high degree of local cortical inhibition and are eventually transformed into interictal spikes on release from inhibition. Earlier studies of spindlelike oscillations in neocortical pyramidal neurons revealed the presence of phasic hyperpolarizing events (Creutzfeldt et al. 1966) during which the probability of antidromic invasion decreased (Jasper and Stefanis 1965), but the properties of inhibitory postsynaptic potentials (IPSPs) were not explored. On the basis of experimental evidence, including extracellular recordings during natural sleep of behaving primates (Steriade 1974) and multisite intracellular and extracellular recordings in anesthetized cats (Steriade and Amzica 1994; Steriade and Contreras 1995), we concluded that the neocortex has a leading role in promoting SW seizures.

Here we show the role of local cortical inhibition in controlling the behavior of pyramidal cells on synchronized thalamic inputs during spindle oscillations. To search for a role of cortical inhibition in controlling the behavior of pyramidal neurons, an immediate approach would be the use of the γ-aminobutyric acid-A ($GABA_A$) blocker bicuculline. However, this procedure is not appropriate because it readily induces epileptic patterns, changing the state of the network and the balance of inputs to pyramidal cells that become dominated by corticocortical inputs (Steriade et al. 1997; D. Contreras and M. Steriade, unpublished data). Therefore we combined in vivo intracellular recordings with computational models to investigate the role and amount of inhibition in pyramidal cells in response to synchronized thalamic inputs during spindles. Recordings with chloride-filled pipettes and dual simultaneous impalements suggest that a large amount of GABAergic inhibition is indeed triggered by thalamic inputs. Staining of the recorded cells, reconstruction, and

0022-3077/97 $5.00

building of computational models allowed us to estimate the amount of inhibitory currents accompanying synchronized inputs of thalamic origin.

METHODS

Experiments were conducted on 25 adult cats under barbiturate anesthesia (35 mg/kg ip). After animals reached the state of deep anesthesia, they were paralyzed with gallamine triethiodide and artificially ventilated with control of the end-tidal CO_2 concentration of ~3.7%. Body temperature was maintained at 37°C and heart beat was continuously monitored (rates between 90 and 110 bpm). Saline glucose was supplemented as a fluid therapy two or three times during the experiment. Deep anesthesia was maintained by additional doses of pentobarbital sodium and by monitoring the EEG to obtain a stable state of spontaneous spindle oscillations. To improve stability of intracellular recordings, bilateral pneumothorax was performed as well as drainage of the cisterna magna and hip suspension. After the pipettes were placed over the surface of the cortex, the hole made for recording was filled with a 4% agar solution. All pressure points and wounds were generously infiltrated with lidocaine.

Intracellular recordings were performed with glass micropipettes filled with one of three different solutions: 3 M potassium acetate (KAc), 3 KCl, or 2 M KAc and 2% Neurobiotin. Pipettes had final DC resistances of 30–40 MΩ. To perform intracellular recordings, the bone and dura overlying the postcruciate gyrus or the anterior part of the suprasylvian gyrus were removed and the exposed cortex was bathed in mineral oil to prevent desiccation. The depth of the pipette was read on the scale of the micromanipulator. Positions of stained neurons indicated that reading error was <15%.

EEG was recorded with coaxial electrodes; the concentric ring (pial surface) and tip (depth) were separated by 0.6 mm, each being exposed for 0.15–0.2 mm. EEG recording electrodes were positioned in the vicinity (~1 mm) of the intracellular recording sites.

Stimulation was applied through similar types of coaxial electrodes inserted in the ventroposterior (VP) or lateroposterior thalamic nuclei according to the cortical area under study.

A high-impedance amplifier (band pass 0–5 kHz) with active bridge circuitry was used to record and inject current into the cells. Signals were recorded on an eight-channel tape (band pass 0–9 kHz) and digitized at 10 kHz for off-line computer analysis.

At the end of experiments, animals received a large doses of Nembutal and were perfused transcardially with physiological saline followed by 10% paraformaldehyde. The brain was removed and stored in Formalin with 30% sucrose. When the brain sank, 80-μm sections were made and processed with the avidin-biotin standard kit, mounted on gel-dipped slides, and coverslipped.

Computational models

MORPHOLOGY. Simulations of neocortical layer V and VI pyramidal cells were based on computerized cellular reconstructions (Eutectic tracing system) of two neurons recorded simultaneously and stained during the present experiments (see Fig. 5). The geometries were incorporated in the NEURON simulation program (Hines 1993) and converted into multicompartment geometries (529 and 198 compartments for layer V and VI cells, respectively) constrained by a minimal dendritic length of 50 μm. Simulations based on more precise digitization of the morphology gave similar results.

CORRECTION FOR SPINES. Layer V and VI neocortical pyramidal cells have a high density of dendritic spines, in the range of 8,000–14,000 spines per cell (Larkman 1991). This represents ~25–45% of the total cell surface (Mungai 1967; see also DeFelipe and Fariñas 1992). Thus, in the model, the dendritic surface was corrected by assuming a uniform spine density that increased the dendritic surface by 45% (~30% of the cell surface). Surface correction was made by rescaling the size of each compartment or by rescaling the values of the specific membrane capacitance (C_m) and conductances in dendrites by a factor of 1.45. Both methods gave similar results.

AXON. The axon hillock and initial segment were modeled with the use of a single equivalent cylinder for each, the size of which was based on serial electron microscopic measurements of neocortical pyramidal cells (Fariñas and DeFelipe 1991b). A more detailed model of pyramidal cells' axons (Mainen et al. 1995) was also used and gave similar results.

PASSIVE PARAMETERS. The passive parameters were estimated by fitting the model to passive voltage traces of injection of small hyperpolarizing current pulses obtained from the same cells. The fit was performed with the use of a simplex fitting algorithm (Press et al. 1986). For a given cellular geometry and assuming uniform passive properties (leak currents, C_m, and specific intracellular resistivity) in the soma and dendrites, multiple solutions were possible. Thus the fit was further constrained by forcing C_m to a value of 1 $\mu F/cm^2$. The fitting procedure then converged to a unique set of passive parameters from different initial conditions. Several combinations of geometry and passive parameters were considered and gave similar results.

ACTIVE MEMBRANE PROPERTIES. Active currents were inserted into the soma, dendrites, and axon with different densities in accordance with available biophysical evidence. In light of patch-clamp data showing that the soma and dendrites of neocortical and hippocampal pyramidal cells have similar Na^+ channel densities (Huguenard et al. 1989; Magee and Johnston 1995; Stuart and Sakmann 1994), the Na^+ conductance was set to 70 $pS/\mu m^2$ (range tested: 20–100 $pS/\mu m^2$) in dendritic and somatic compartments. This value corresponds to the estimated value for Na^+ current (I_{Na}) densities in adult pyramidal neurons of the hippocampus. Axonal densities used were in agreement with binding and immunohistochemical studies (Black et al. 1990), indicating that there is a much higher Na^+ channel density in the initial segment and nodes of Ranvier compared with the internodal, somatic, and dendritic membranes. A density of Na^+ channels of 30,000 $pS/\mu m^2$ was chosen for the axon initial segment and nodes of Ranvier. This high density was required to reproduce the overshooting somatic action potentials observed in most in vivo intracellular recordings while being consistent with the density of the order of 70 $pS/\mu m^2$ in soma and dendrites. This value falls within the range of estimated Na^+ channel density in the axon (Black et al. 1990) and is also in agreement with a recent model of the axon (Mainen et al. 1995). The Na^+ channel density of the internodal segments was set at the same value as the soma and dendrites. High-threshold Ca^{2+} currents (I_{CaL}) were inserted in dendrites (30 $pS/\mu m^2$ in most proximal regions up to 50 μm from soma, and 15 $pS/\mu m^2$ elsewhere) and soma (30 $pS/\mu m^2$) according to the densities estimated in hippocampal pyramidal cells by patch-clamp recordings (Magee and Johnston 1995). The delayed-rectifier potassium conductance (I_{Kd}) was inserted with a density of 100 $pS/\mu m^2$ in dendrites and 200 $pS/\mu m^2$ in soma (tested range: 20–300 $pS/\mu m^2$). In the axon initial segment and nodes of Ranvier, a density of 2000 $pS/\mu m^2$ was used. A noninactivating K^+ conductance (I_M) was also included in the soma and dendrites with a density of 5 $pS/\mu m^2$. This value was required to reproduce the repetitive firing behavior of neocortical pyramidal neuron observed in vivo.

KINETICS OF INTRINSIC CURRENTS. I_{Na}, I_{CaL}, I_{Kd}, and I_M were described by Hodgkin-Huxley-type equations (Hodgkin and Huxley 1952) and were solved with the use of NEURON (Hines 1993).

Kinetics for I_{Na} and I_{Kd} were taken from models of hippocampal pyramidal cells (Traub and Miles 1991) with reversal potentials of +50 and −90 mV, respectively. Previous models of neocortical pyramidal cells were used for the kinetics of I_{CaL} (Reuveni et al. 1993) and I_M (Gutfreund et al. 1995). Intracellular Ca^{2+} dynamics was modeled in a 0.1-μm shell beneath the membrane (see Destexhe et al. 1993): influx of Ca^{2+} occurred through Ca^{2+} channels and Ca^{2+} efflux was a fast-decaying signal (time constant of 5 ms) to an equilibrium intracellular Ca^{2+} concentration of 240 nM. The extracellular Ca^{2+} concentration was kept at 2 mM and the Ca^{2+} reversal potential was calculated with the use of the Nernst relation (equilibrium reversal potential of about +120 mV). All simulations corresponded to a temperature of 36°C (temperature factor for time constants was $Q_{10} = 3$).

KINETICS OF SYNAPTIC CURRENTS. Alpha-amino-3-hydroxy-5-methyl-4-isoxalone proprionic acid (AMPA), *N*-methyl-D-aspartate (NMDA), and $GABA_A$ receptors were modeled with the use of two-state kinetic models (Destexhe et al. 1994, 1996). Other types of synaptic responses were not included because they were not required to account for the behavior of the cells and also because GABAergic and glutamatergic synapses account for the vast majority of synapses in the cerebral cortex (White 1989; DeFelipe and Fariñas 1992). On the basis of whole cell recordings of hippocampal pyramidal and dentate gyrus cells (Hessler et al. 1993; Otis and Mody 1992; Xiang et al. 1992), kinetic models of $GABA_A$, NMDA, and AMPA receptors were fit to experimental data with the use of a simplex procedure (see details in Destexhe et al. 1996).

RESULTS

Data base and cellular identification

The present results were obtained from 63 cortical cells intracellularly recorded from layers II to VI within the primary somatosensory cortex (SI) in the postcruciate gyrus or in the association area 5 of the anterior suprasylvian gyrus. The cells were identified by antidromic and/or orthodromic responses to VP or lateroposterior thalamic stimulation. Of those 63 cells, 34 were recorded in pairs ($n = 17$), with both simultaneously recorded cells located either in SI ($n = 8$) or area 5 ($n = 9$). In six pairs, pipettes contained KAc in one cell and KCl in the other. In seven pairs, Neurobiotin 3% was added to the pipette solution (KAc). Two cells of a pair recorded from SI were reconstructed and used for the simulations presented here. Cortical cells had a stable resting membrane potential (V_m) of −72 ± 1.8 (SE) mV and overshooting action potentials of 79.3 ± 2.1 mV. Input resistance measured with short squared hyperpolarizing pulses was 19.4 ± 2.2 MΩ. All cells included in this study were of the regular spiking type (Chagnac-Amitai et al. 1990; Connors et al. 1982; McCormick et al. 1985; Nuñez et al. 1993).

Presence of IPSPs during spindling

The first test for the presence of inhibitory events during spindle oscillations in cortical neurons was the application of different DC levels ($n = 48$). Figure 1 shows an example of an SI cell under hyperpolarizing DC (Fig. 1*A*, *left*, −80 mV), displaying depolarizing potentials at 7 Hz, in phase with spontaneous spindle waves recorded from the cortical depth in the vicinity of the cell. The resting V_m was −69 mV. On DC depolarization (Fig. 1*A*, *left*, −60 mV), the presence of IPSPs was revealed within spindle sequences, occurring concomitantly with EPSPs that occasionally led to spike firing. To study the shape of synaptic events during spontaneous spindle sequences, the negative peaks of the depth-recorded EEG were taken to indicate *time 0* and the intracellular traces were aligned to those marks (Fig. 1*A*, *right, time 0* indicated by vertical dotted line). Superimposition of several spindle waves showed that the depolarizing postsynaptic potentials (PSPs) (Fig. 1*A*, *right*, −80 mV, $n = 10$) had durations similar to those of the individual EEG waves (~0.12 s), with coincident peaks of maximum amplitude. The intracellular potentials showed an additional low-amplitude (2–3 mV) tail lasting almost 50–60 ms. Depolarizing the cell with DC (Fig. 1*A*, *right*, −60 mV, $n = 10$) demonstrated that the second half of the spindle-related PSPs was dominated by IPSPs that followed the EPSPs (the latter prevailed during the 1st half of the EEG spindle waves). The IPSPs shown in Fig. 1 had amplitudes of 8 mV and durations of ~0.1 s at −60 mV. IPSPs reversal was −70 mV.

In a sample of 37 cells, the amplitude of IPSPs associated with spindling was 7.4 ± 1.4 (SE) mV and the duration was 81.2 ± 8.1 ms, both measured at −54 mV under depolarizing DC. The reversal of the IPSPs was at −69.4 ± 3.2 mV, with the result that most of them were reversed at resting conditions. The variability of the reversal and other IPSP values is due to their compound nature and the unavoidable mixture with EPSPs. We did not observe a significant variation of IPSP amplitude or duration between cortical regions. After Cl^- infusions ($n = 23$), strong depolarizing potentials associated with spindling inputs developed after >10 min in 90% of cells ($n = 20$), with amplitude of 38.1 ± 7.6 mV and duration of 98.3 ± 13 ms, both measured at the resting V_m.

That spindle-related IPSPs were indeed triggered by thalamic inputs was shown by comparing the shape and behavior, at different V_ms, of spontaneously occurring IPSPs during spindling with those evoked by thalamic stimulation. Figure 1*B*, *left*, shows that VP stimulation triggered an EPSP in an SI neuron, followed by an IPSP under DC depolarization (−57 mV); the latter was completely reversed by DC hyperpolarization (−80 mV). The same behavior to current injection was found for the IPSPs occurring during spontaneous spindle sequences (Fig. 1*B*, Spontaneous), with a reversal at around −70 mV. At rest (*middle traces*) spontaneous PSPs were barely visible, but thalamic stimulation revealed a clear EPSP/IPSP sequence. During spontaneous spindle waves, excitation in cortical neurons was less powerful than that elicited by thalamic stimulation, but the IPSPs looked almost identical.

The thalamic-evoked early EPSP/IPSP response was followed by a spindle sequence after ~0.1 s (Fig. 2). Both the initial synaptic response and the subsequent oscillatory event showed a similar behavior to injected current. At rest (Fig. 2, *top*, −70 mV) there were depolarizing responses, whereas under DC depolarization (−55 mV) the responses were reversed, thus showing that most of the VP-evoked response was an IPSP. Hyperpolarization to −80 mV, by means of DC injection, increased the amplitude of the reversed IPSPs. A similar behavior was seen during spontaneously occurring

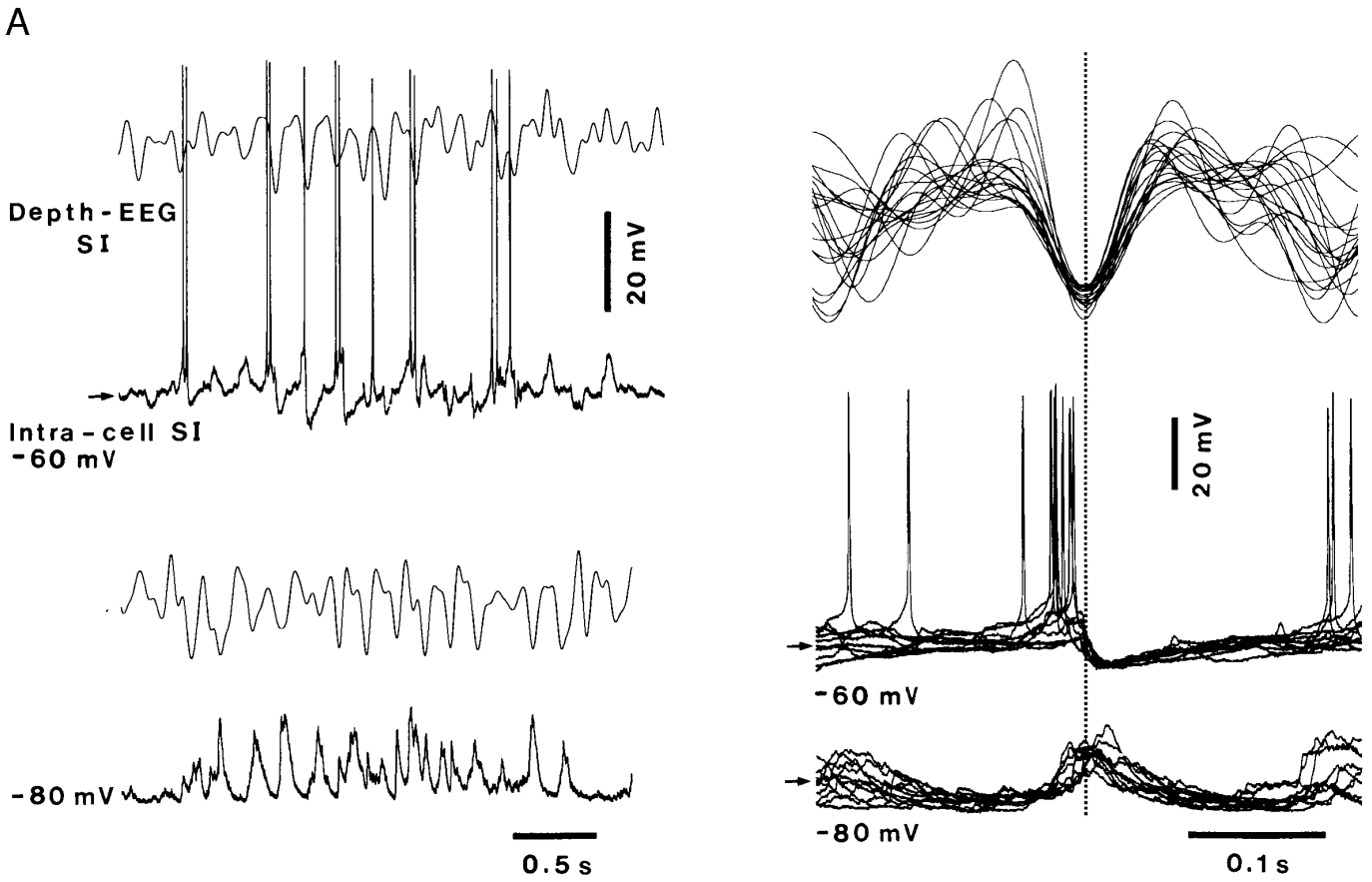

FIG. 1. Participation of inhibitory postsynaptic potentials (IPSPs) in cortical spontaneous spindles. *A, left*: examples of spindle sequences under barbiturate anesthesia in a neuron from primary somatosensory cortex (SI), recorded together with depth electroencephalogram (EEG) from its vicinity (Depth-EEG SI). *Top traces* were under depolarizing DC (−60 mV) and *bottom traces* under DC hyperpolarization (−80 mV). *A, right*: superimposed traces [10 cycles for each membrane potential (V_m)] are from successive cycles of same cell, at −60 and −80 mV; traces were aligned to negative peaks of depth EEG (*top traces*, $n = 20$; *time 0* indicated by vertical dotted line; 10 sweeps correspond to intracellular recording at −60 mV, remaining 10 sweeps to −80 mV; note stable EEG spindles in both cases). *B*: different SI cell responded to ventroposterior (VP) stimulation (Thalamic stimulation, ●) while V_m was changed by means of DC (resting $V_m = -70$ mV; 2 traces superimposed for each stimulus). VP-evoked responses were compared with spontaneous postsynaptic potentials (PSPs) during spindling, aligned by depth EEG peak negativities (Spontaneous; EEG was not depicted; see *A*) and under similar DC levels as for VP-evoked responses.

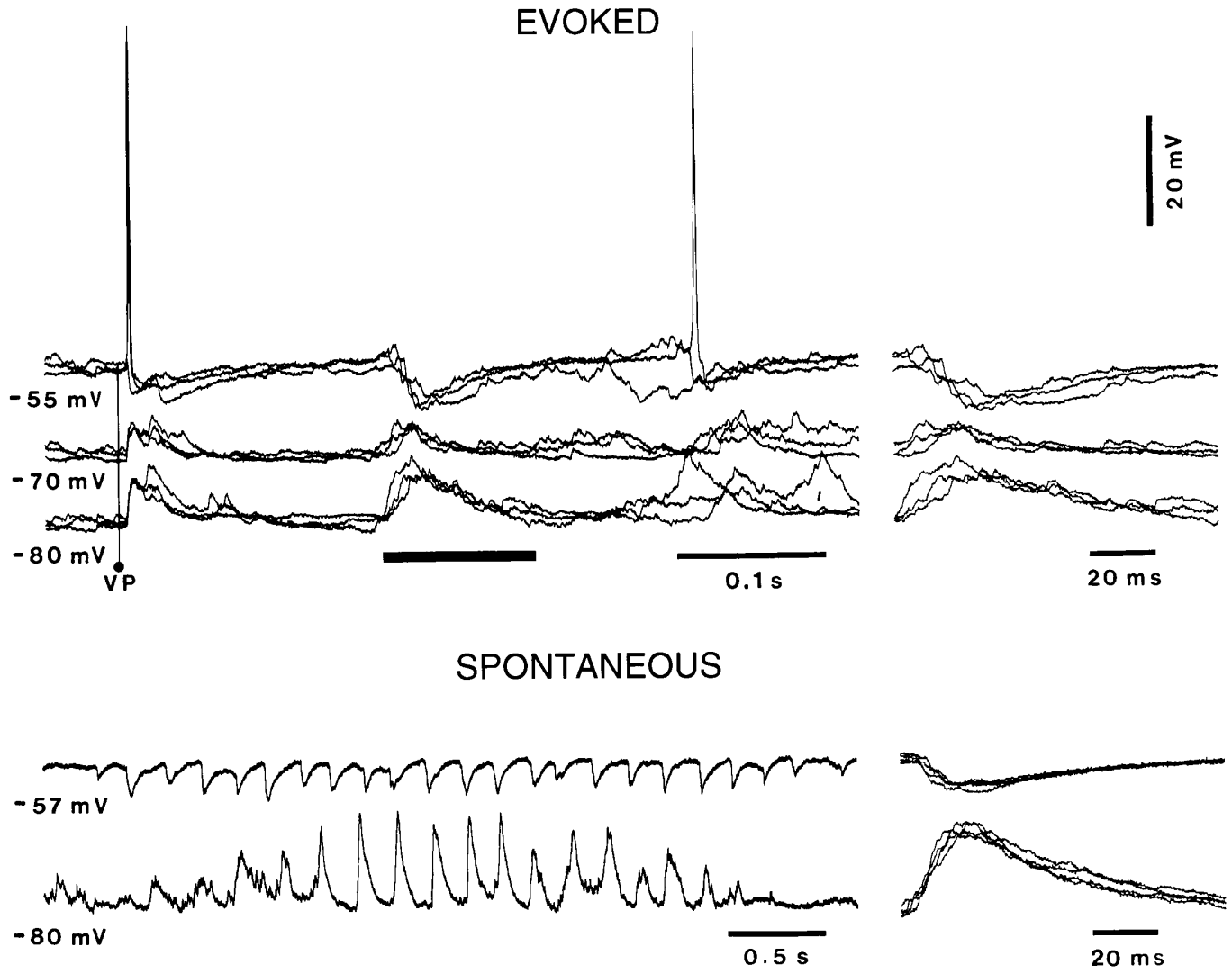

FIG. 2. Similar IPSPs are present in thalamic-evoked and spontaneous spindle oscillations. *Top*: superimposed traces (3 traces for each V_m) from successive responses to VP stimulation (●) while V_m was changed with DC (V_m = −70 mV). Black bar: 1st cycle of evoked spindle sequence (expanded at *right*). *Bottom*: spontaneous spindle sequence from same cell in which spindle-related PSPs were depolarizing under DC hyperpolarization (−80 mV) and were reversed by DC depolarization at −57 mV. Some spontaneous IPSPs from depicted sequence are expanded and superimposed (n = 4) at *right* to illustrate similarity with evoked IPSPs.

spindles; when the cell was depolarized with DC injection (Fig. 2, *bottom*, −57 mV), the oscillatory events were almost exclusively constituted by IPSPs, whereas under DC hyperpolarization (−80 mV) they were completely reversed, similarly to the synaptic events in the evoked spindling (the amplitude and time course of evoked and spontaneous synaptic events are shown in the expanded and superimposed traces in Fig. 2, *right*). In both spontaneous and evoked spindling shown in Fig. 2, IPSPs had amplitudes of ~5 mV at −55 mV and ~10 mV when inverted at −80 mV, and they lasted from 65 to 80 ms.

Intracellular chloride injection

To reveal the amount of Cl^- GABAergic inhibition during each cycle of a spindle oscillation, cortical cells from SI and anterior suprasylvian area 5 were recorded with KCl-filled pipettes (n = 23). The injection of Cl^- ions into the cells is expected to shift the reversal potential for Cl^--mediated $GABA_A$ responses to more positive values. Shortly after impalement, cells that previously fired scattered single action potentials during spindling started to fire one to three action potentials per spindle wave on the top of growing depolarizing potentials, in phase with the depth EEG recorded from the vicinity (Fig. 3, 1′ after impalement). After a few minutes (Fig. 3, 10′ after impalement), the cell was firing bursts of four to seven action potentials at 100 Hz with spike inactivation, resembling PDS, in phase with spindle waves.

To verify whether the increased amplitudes and duration of PSPs, produced by the leakage of Cl^- inside the cell, were confined to a certain phase of the spindle oscillatory cycle, we compared the changing PSPs with the EEG activity from the cortical depth. Figure 3, *top trace at right*, illustrates

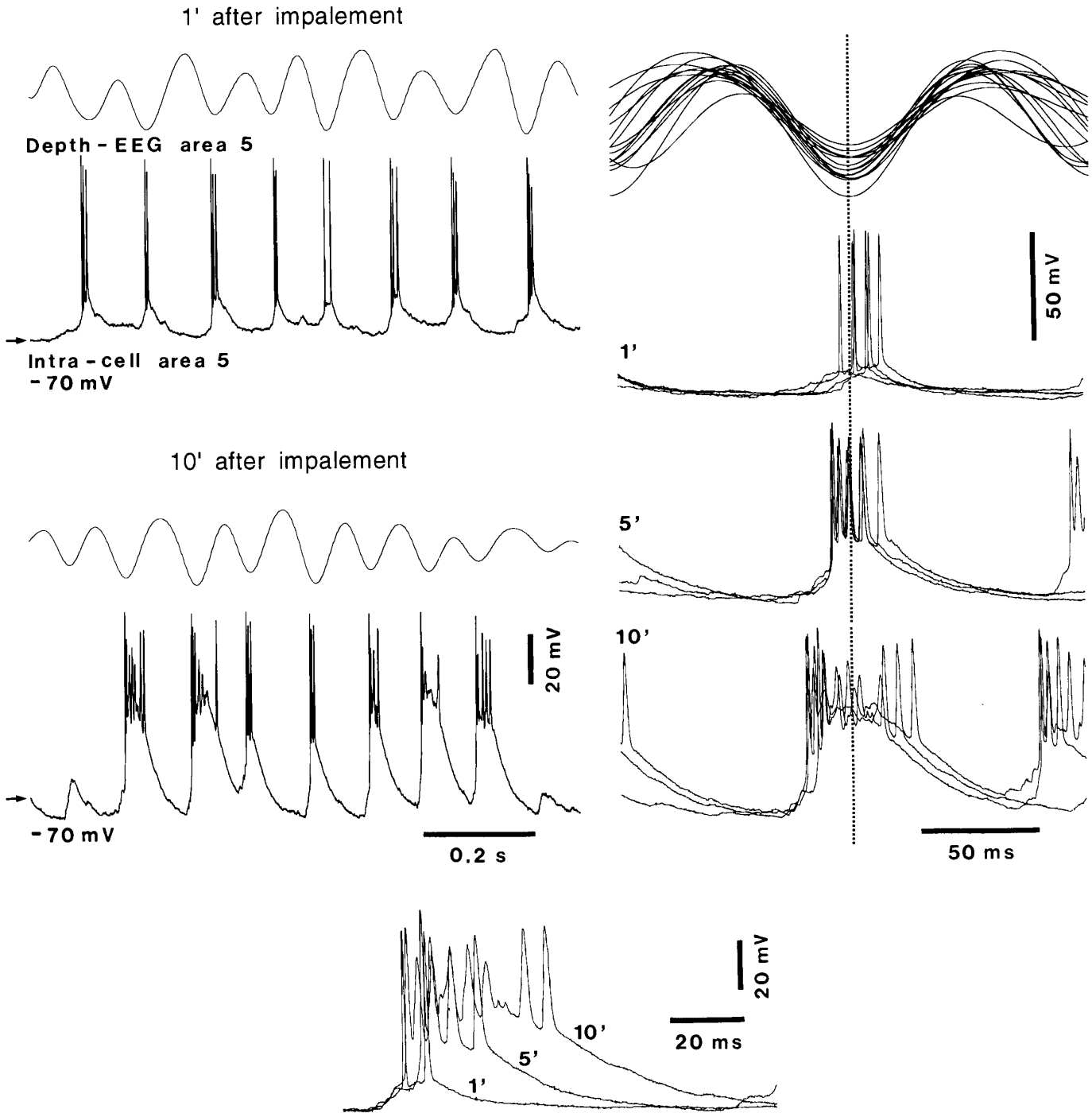

FIG. 3. Spindle-related inputs to cortical cells are embedded in Cl^--mediated GABAergic inhibition. A cortical cell from suprasylvian gyrus (area 5) was recorded with a pipette loaded with KCl (3 M) at rest (−70 mV), simultaneously with EEG from its vicinity (Depth-EEG area 5). *Left*: 2 spontaneous spindle sequences at 1 min (*top*) and 10 min (*bottom*) after impalement. *Right*: superimposed individual spindle waves recorded at 1, 5, and 10 min after impalement; alignment to negative peak of depth EEG (vertical dotted line). *Bottom*: 3 individual spindle waves from superposition at *right*, aligned by their initiation times.

superimposed oscillatory cycles taken from spontaneous spindle sequences occurring at different times after the impalement. The negative peak of the depth EEG was taken as reference time for the alignment of the intracellular traces. An increased duration and amplitude appeared uniformly at both sides of the center line, showing that although IPSPs usually dominated the second half of spindle-related synaptic events, they were present from the beginning of each oscillatory cycle. Spindle-related depolarizing potentials progressively changed from 7–8 mV in amplitude and 30 ms in

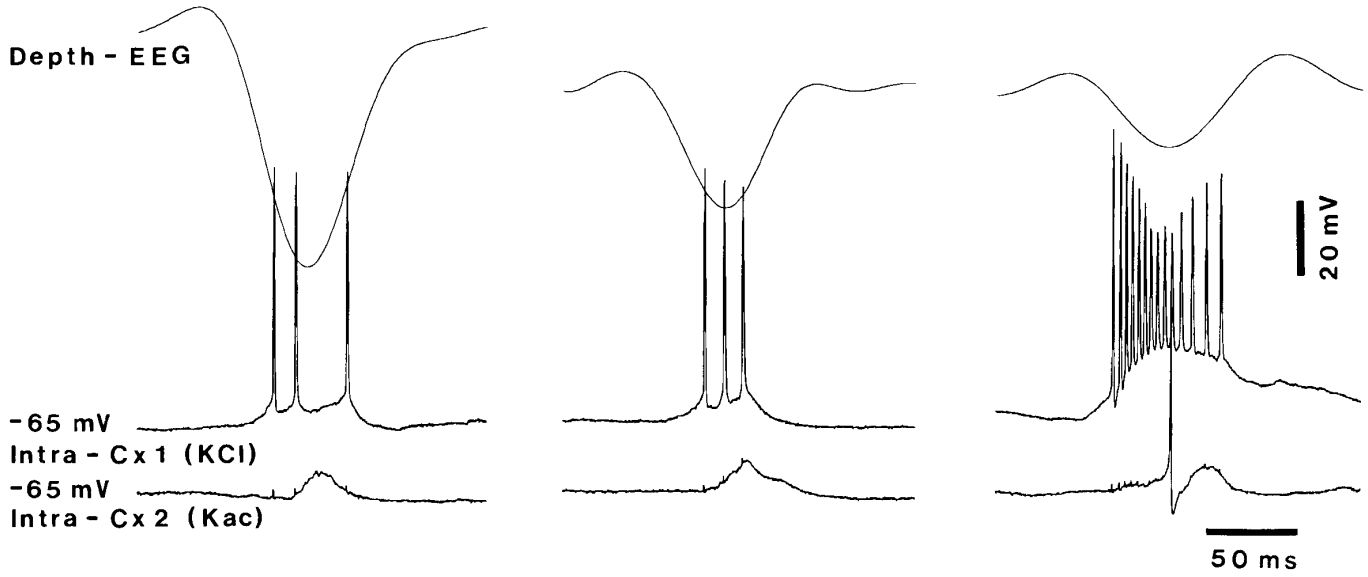

FIG. 4. Comparison of spindling inputs to 2 simultaneously recorded cortical cells. Two cells from area 5, separated by 3 mm, were simultaneously recorded at rest (−65 mV), together with depth EEG between 2 pipettes (Depth-EEG). Cx 1 cell was recorded with pipette containing 3 M KCl; recording pipette for Cx 2 cell contained 3 M potassium acetate (KAc). Shown are 3 examples of spontaneous individual spindle waves in which intracellular potential in Cx 1 was of higher amplitude than in Cx 2. Here and in Fig. 5, small deflections in 1 cell that are simultaneous with full action potentials in another cell are effects of capacitive coupling.

duration (Fig. 3, *right,* 1′ after impalement) to 25 mV and 50 ms (5′), finally reaching values of up to 45 mV in amplitude and 100 ms in duration (10′). These alterations were observed without changes in the resting V_m (−70 mV). A superposition of individual spindle-related synaptic potentials at 1, 5, and 10 min after impalement is illustrated in Fig. 3, *bottom.* The traces were artificially aligned by the time of departure from baseline.

Dual simultaneous intracellular recordings

Spindle oscillations are preferentially distributed to the pericruciate and suprasylvian cortex (Morison and Dempsey 1942) and they are nearly simultaneous throughout the suprasylvian gyrus during both barbiturate anesthesia and natural sleep in cats and humans (Contreras et al. 1996, 1997). Therefore similar thalamic inputs are shared by an important number of cortical cells. This prompted us to study the effect of Cl^- injection in one cell while recording another cell with KAc solution as a control reflecting the state of the network during spindle-related inputs. We performed dual simultaneous impalements of neurons separated by 1–3 mm in suprasylvian area 5 ($n = 8$) or SI cortex ($n = 7$). During the same cycle of spindle oscillation, synaptic potentials were of higher amplitude in the cell recorded with KCl (Fig. 4, Cx 1) compared with the cell recorded with KAc (Fig. 4, Cx 2).

Although TC excitation is synchronized over large cortical territories during spindling, the inhibitory inputs that control spindle-related excitatory events are presumably generated locally. We tested this possibility by performing dual intracellular recordings as indicated above, but with both pipettes containing KAc as well as Neurobiotin ($n = 5$ pairs) to reveal the position and morphology of the cell and to allow the construction of realistic computer models. Figure 5*A* shows an example of two pyramidal cells from SI, recorded and stained simultaneously. The cell in Fig. 5*A, left,* was located in upper layer V, with a pyramidal-shaped soma and a prominent apical dendrite that bifurcated early, giving rise to three trunks that ramified in layer I (see reconstruction in Fig. 6). Basal dendrites from this layer V cell ramified extensively into layers V and VI. The cell in Fig. 5*A, right,* was located in layer VI; it had an ovoidal soma with a thin apical dendrite that did not reach layer I, and two prominent basal dendritic trunks, one of them coursing far into the white matter. The two cells (Fig. 5*B, cell 1* = layer VI, *cell 2* = layer V) showed a mixture of PSPs leading to occasional firing during synchronized spindle oscillations in the EEG from the vicinity of *cell 1.* Single, high-amplitude IPSPs, occurring in relation to spindle waves, were confined to one of the two cells at a time (Fig. 5*C*). In Fig. 5*C, left,* the EEG from the vicinity of *cell 1* shows two cycles of a spindle oscillation in which both cells displayed synchronized PSPs leading to spike firing, but only *cell 2* displayed a clear IPSP following the excitatory potential that was synchronized with *cell 1.* In Fig. 5*C, right,* it was *cell 1* that displayed a high-amplitude IPSP, corresponding to the depth EEG spindle wave. This result indicates that, although synchronized excitatory inputs from thalamic bursts trigger inhibition concomitantly in virtually all cortical targets, the machinery responsible for the inhibition is local and is able to generate slight differences among various sites in the circuit.

Computational models

We next explored the possibility that feedforward inhibition in the dendritic shafts close to the soma, triggered by thalamic inputs (see shaded areas in the scheme of

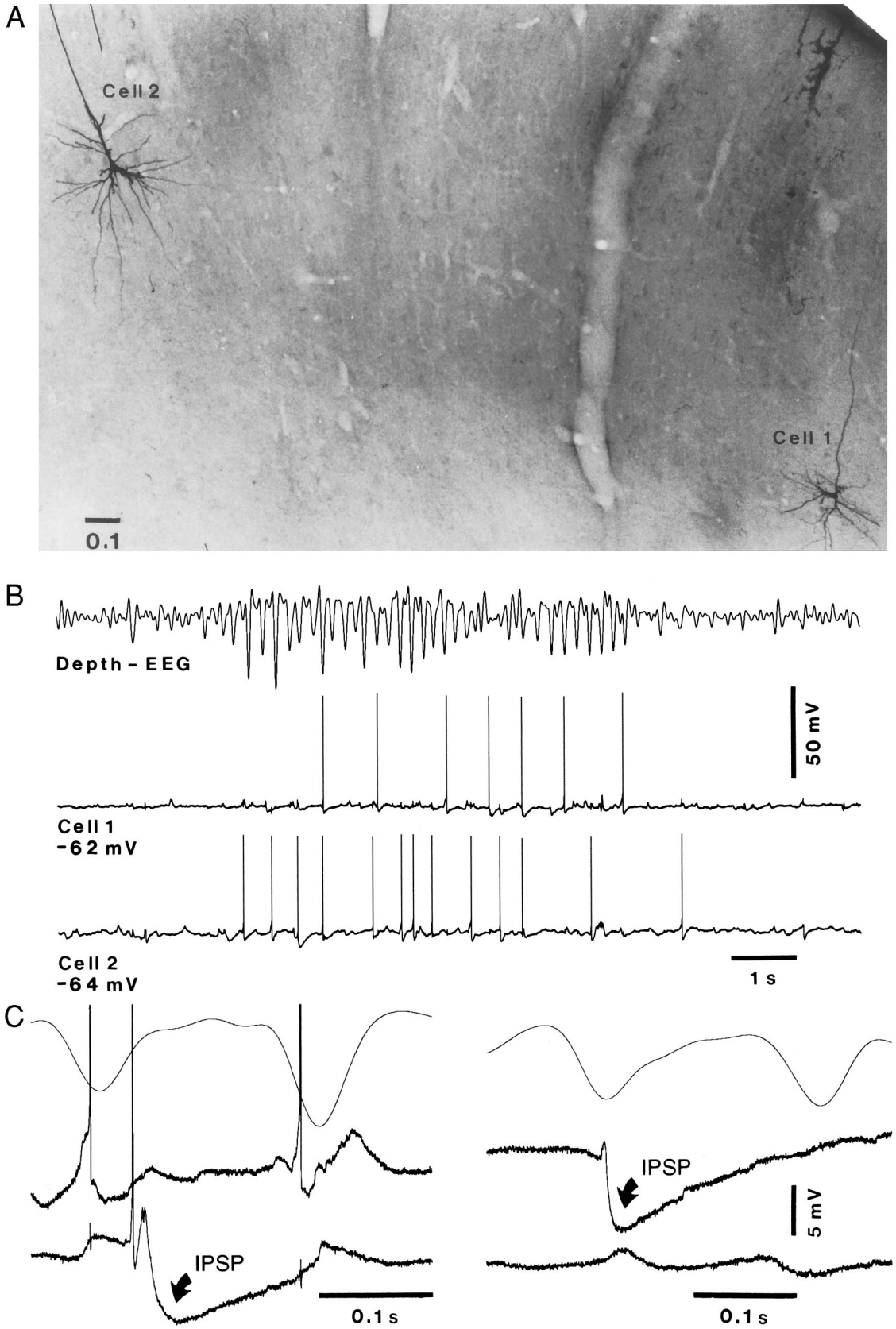

FIG. 5. Inhibition associated with spindling inputs is generated locally. *A*: 2 cells were recorded simultaneously from postcruciate SI cortex with pipettes containing Neurobiotin 2%. Both were found on same section: *cell 1* (*right*) was in layer VI and *cell 2* was in layer V. *B*: example of a spontaneous spindle sequence in both cells. Depth EEG recorded from vicinity of *cell 1*. *C*: two individual spindle waves from a different sequence as shown in *B*, showing IPSP visible only in *cell 2* (*left*, ↓) and in *cell 1* (*right*). Depth EEG recorded from vicinity of *cell 1*.

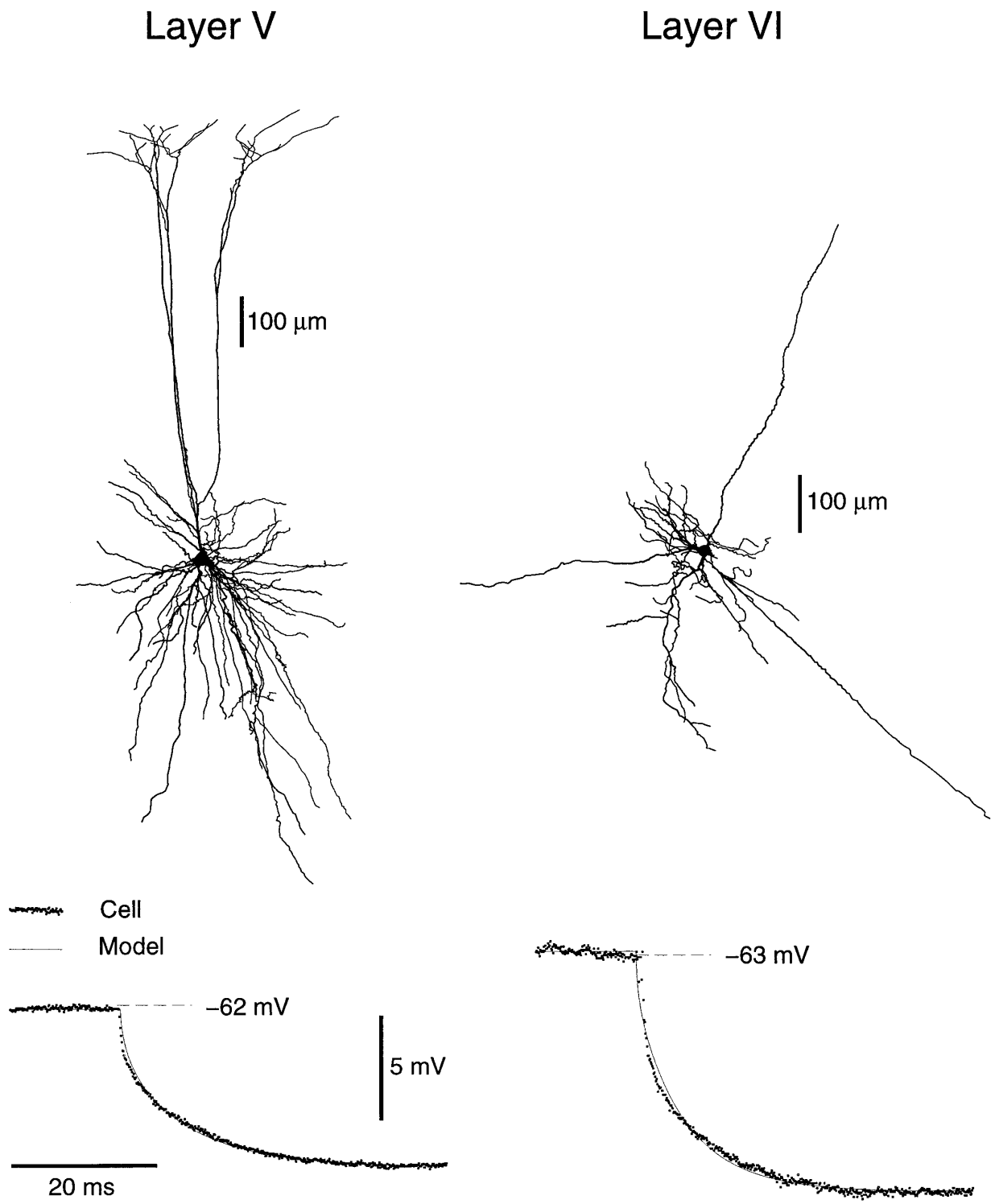

FIG. 6. Geometry and passive properties of simulated cortical pyramidal cells. Two cortical cells illustrated in Fig. 5*A* were reconstructed with the use of a tracing system. Layer V cell had 9 primary branches with a total dendritic length of 22,173 μm^2 and a total area of 91,620 μm^2. In layer VI cell, these parameters were 7,576 and 31,225 μm^2, respectively. Geometry of these cells was incorporated in the NEURON simulation environment and model parameters were adjusted to recordings of specific cells that were stained, based on passive responses to hyperpolarizing current pulses (*bottom*). Optimal parameters of layer V cell: leak conductance, 0.097 mS/cm^2; leak reversal, −61.2 mV; axial resistance, 384 Ω/cm for a specific capacitance of 1 $\mu F/cm^2$. Optimal parameters of layer VI cell: leak conductance, 0.13 mS/cm^2, leak reversal, −63.25 mV, axial resistance, 184 Ω/cm for a specific capacitance of 1 $\mu F/cm^2$.

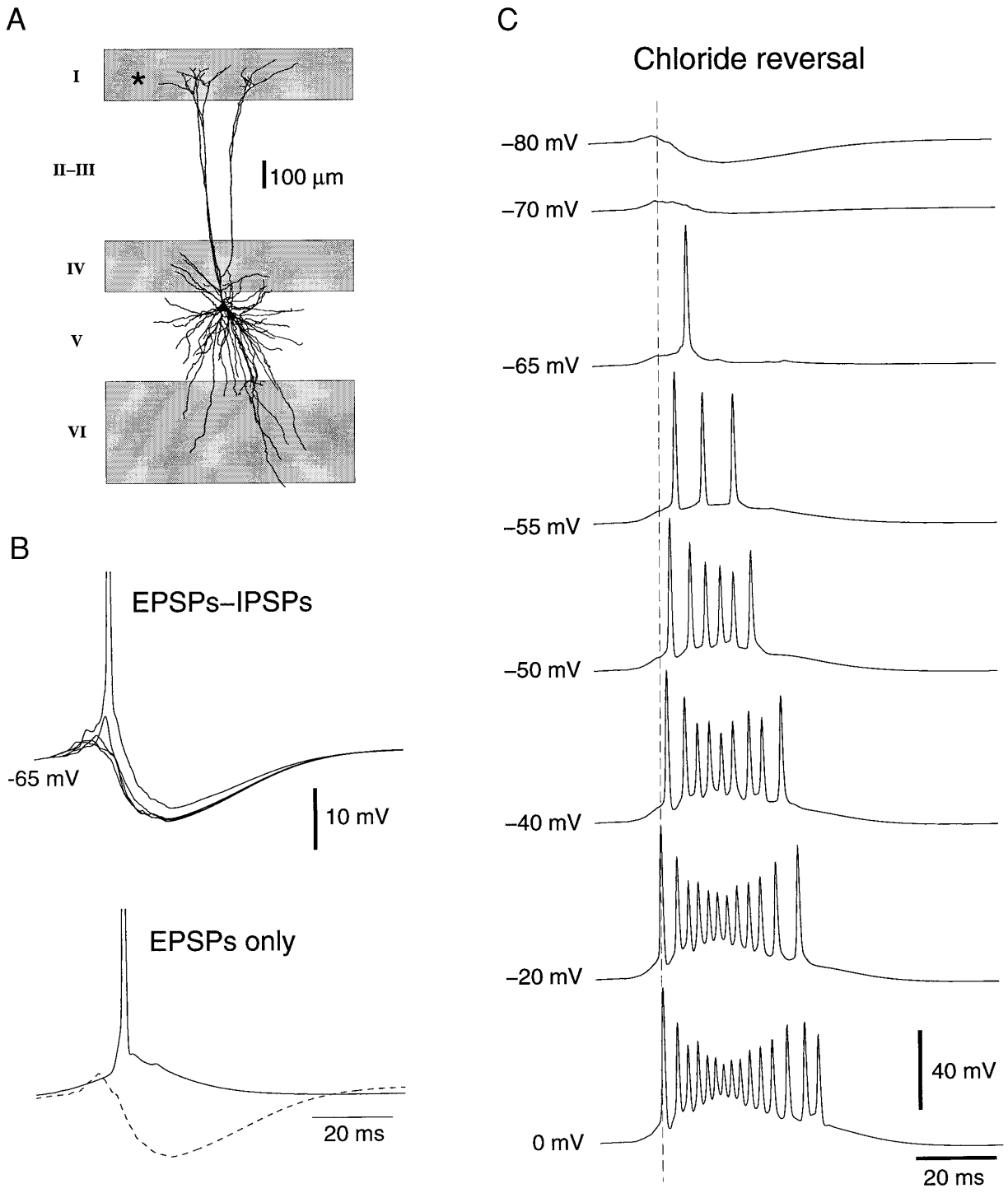

FIG. 7. Simulation of PSPs and evoked bursts following thalamic stimulation. *A*: distribution of direct excitatory inputs in layer V pyramidal cell. Shaded area: limits of cortical layers I, IV, and VI, in which excitatory inputs were simulated in cell. Inhibitory inputs were simulated in all layers, with a higher density in soma and proximal dendrites. *B*: simulated excitatory PSP (EPSP)/IPSP sequence following synaptic activation. *B, top*: 3 superimposed responses of cell, which occasionally led to firing (spike truncated) in ~3% of cases. *B, bottom*: response of cell to same EPSPs, in absence of IPSP, led to firing in 95% of cases. *C*: progressive shift in reversal of chloride ions changed response of cell from EPSP/IPSP sequence (−80 mV) to shunting response (−70 mV), and gradually larger EPSPs and bursts of action potentials with spike inactivation.

Fig. 7), could account, if inverted by chloride injection, for the PDS-like potentials in the recordings shown above. We constructed realistic computer models from the two cells depicted in Fig. 5. The traced neurons and the fitting of their passive properties are shown in Fig. 6. Models were aimed at estimating the ratio of excitation/

inhibition needed to account for bursts of action potentials.

Figure 6 shows the reconstructed geometries of two cortical neurons recorded simultaneously and filled with Neurobiotin (as in Fig. 5). Passive parameters were estimated by fitting directly the model on the basis of these geometries to the experimental recordings obtained in the same two cells (Fig. 6, *bottom*). This procedure was followed for each cell and provided an estimate of passive parameters compatible with cellular recordings (see METHODS). In particular, the simulated neuron had input resistance and time constant values very close to those estimated from intracellular recordings. Active properties were based on recent models of action potential generation in pyramidal cells that included dendritic I_{Na} (Mainen et al. 1995; Paré et al. 1997) (see details in METHODS).

Synaptic responses in pyramidal cells following cortical stimulation were successfully modeled on the basis of morphological and electrophysiological constraints (Paré et al. 1997). In that case, a pyramidal cell model could reproduce the amplitude, rise time, specific intracellular resistivity change, and reversal potential of EPSP/IPSP sequences evoked by cortical stimuli at different depths (Paré et al. 1997). In the present case, we used a similar approach to simulate EPSP/IPSP sequences in pyramidal cells following thalamic stimulation, based on the following constraints. *1*) Ultrastructural data on distribution and density of synapses on pyramidal cells constrain the amount of available synapses in different regions of the dendritic tree. *2*) The arborization patterns of TC fibers in cortex constrain the localization of synaptic currents activated by a given stimulus. *3*) Electrophysiological features of the responses of pyramidal cells to thalamic stimulation in normal and reversed-IPSP conditions constrain the amplitude of synaptic currents. These three points are considered in more detail below.

1) Morphological data show that the relative density of glutamatergic and GABAergic terminals in different regions of pyramidal cells follows general rules (reviewed in DeFelipe and Fariñas 1992). Electron microscopic observations of neocortical pyramidal cells have established that the soma, most proximal dendritic segments, axon hillock, and initial segment exclusively form symmetric synaptic contacts (Jones and Powell 1970; Peters et al. 1990) that are mainly GABAergic (see DeFelipe and Fariñas 1992; White 1989). Quantitative studies have revealed that the density of symmetric synapses on the soma of deep pyramidal cells is 10.6 + 3.7 per 100 μm^2 (Fariñas and DeFelipe 1991a), whereas the initial segment forms 20–24 symmetric synapses (Fariñas and DeFelipe 1991b). About 16% of the total number of synapses found on neocortical pyramidal cells are of the symmetric variety: 7% of these end on the soma and 93% on the dendrites (DeFelipe and Fariñas 1992). Given that the modeled neuron had a soma surface of 3,200 μm^2 and a dendritic surface of 91,620 μm^2, this yields a ratio of ~2.3:1 in favor of the soma. Thus, in our model, the relative densities of GABAergic synapses were 0.26, 0.6, 2.5, and 2.5 for the dendrites, soma, axon hillock, and initial segment, respectively. In neocortical pyramidal neurons, the vast majority of asymmetric synapses is found on dendritic spines (White 1989). Further, the most proximal dendritic segments (up to 40 μm from soma) are devoid of spines (Jones and Powell 1969; Peters and Kaiserman-Abramof 1970) and mostly form symmetric synapses (Jones and Powell 1970). Thus, in our model, excitatory synapses were exclusively located in the dendrites, with a uniform density, and no excitatory synapses were located in the first 40-μm dendritic segments close to the soma.

2) Having estimated the relative ratios of excitatory and inhibitory terminal density in different regions of the cell, we need further data to determine the absolute amount of synaptic current activated by any given stimulus. If thalamic stimulation is subthreshold in the recorded cell, it is likely to be subthreshold in the majority of pyramidal cells in the neighborhood of the cell. It seems therefore reasonable to assume that the EPSP resulting from thalamic stimulation is essentially due to the direct activation of excitatory synapses by TC fibers, whereas polysynaptic contributions would be negligible. Anatomic data show that thalamic axons end preferentially in layers I, IV, and VI (Herkenham 1980; Jones 1985). On the basis of these data, we have estimated that TC synapses are distributed as follows: 15% in layer I (>800 μm above the soma), 60% in layer IV (from 50 to 200 μm above the soma), and 25% in layer VI (below 200 μm of the soma); no excitatory synapses were stimulated elsewhere. These locations are schematized in Fig. 7*A*.

On the other hand, there are no direct inhibitory inputs following thalamic stimulation in neocortical pyramidal cells. IPSPs therefore occur presumably through the feedforward recruitment of interneurons by TC fibers. Subthreshold thalamic stimulation is indeed likely to fire interneurons because of the higher input resistance of the latter. We have therefore considered that thalamic stimulation activates inhibitory synapses everywhere in the dendritic tree, according to the distribution of densities established by morphological studies (see point 2 above).

The pattern of presynaptic stimulation was determined as follows. We assumed that thalamic stimulation recruits cortical cells through short bursts of high-frequency action potentials. Each excitatory synapse received a burst of randomized presynaptic pulses at an average rate of 300 Hz (range tested: 100–400 Hz) during 10 ms (range tested: 5–20 ms). Inhibitory synapses received a similar presynaptic pattern after a 2-ms delay (range tested: 1–4 ms).

3) The parameters of the model (namely, location, number, strength, and timing of EPSPs/IPSPs) were constrained by recording EPSP/IPSP sequences following thalamic stimulation in KAc- and KCl-filled pipettes. With the ratios of synapses determined in point 1 and the pattern of activation described in point 2, the maximal conductance of excitatory and inhibitory synapses was constrained by the relative amplitude and time course of EPSP/IPSP sequences and by the typical bursts of action potentials induced by thalamic stimuli in Cl-filled pipettes.

In normal conditions (KAc-filled pipettes), subthreshold thalamic stimuli evoke an EPSP followed by an IPSP (see Fig. 1). These conditions could be reproduced by a large range of parameters, provided that EPSPs and IPSPs were delayed by ~2 ms (Fig. 7*B*). However, the possibility remains that the hyperpolarization following the EPSP be explained by the activation of dendritic currents with no sign

of spiking in the soma, such as dendritic calcium-dependent potassium current ($I_{K(Ca)}$) (Lang and Paré 1997; Sah and Bekkers 1996).

The responses of pyramidal cells to the same stimulus intensities, recorded with the use of KCl-filled electrodes, provided more constraints to the model. The same parameters could reproduce the EPSP/IPSP sequence in normal conditions (Fig. 7*B*) and the gradual development of a burst of action potentials with Cl^- ions in the cell (Fig. 7*C*). This constraint narrowed down the range of parameters, allowing us to reproduce these phenomena. It was consistently found that bursts of action potentials, similar to those observed during recordings, are essentially due to the reversal of IPSPs in the somatic region, leading to a powerful inward current near the soma (see also below).

Cl^- ions not only lead to powerful spike bursts, but they also cause a significant phase advance of action potential firing relative to the peak of the field potential (see Fig. 3, *right*). This feature could be reproduced in the model (Fig. 7*C*), assuming that EPSPs and IPSPs do not arrive exactly at the same time at each synapse, leading to a short period of competition between EPSPs and IPSPs in the dendrites. Once IPSPs are reversed, instead of competing against each other, EPSPs and IPSPs summate, thus leading to earlier firing. Assuming that synaptic events occurred with an SD of ~6 ms for EPSPs and 4.5 ms for IPSPs (plus a 2-ms delay), a phase advance of ~10 ms was reproduced (Fig. 7*C*), comparable with experimental data. SDs of 4–6 ms are compatible with the variability of cellular discharges observed in intracellular recordings of cortical and thalamic neurons in vivo, as compared with field potentials (Contreras and Steriade, unpublished data).

The type and localization of currents underlying Cl^- bursts were investigated in the model by adding or removing currents in selected regions of the cells. Suppressing IPSPs in dendrites had minimal effects (Fig. 8*A*), but the burst was highly affected by removing proximal IPSPs (Fig. 8*B*). Removing dendritic Ca^{2+} (Fig. 8*C*) or Na^+ (Fig. 8*D*) currents caused minimal changes. Dendritic EPSPs and IPSPs could not account for the burst (Fig. 8, *E* and *F*), but keeping only proximal IPSPs produced bursts similar to those in the control condition (Fig. 8*G*). Finally, injection of an inward triangular ramp current in the soma led to a burst with very similar morphology as with synaptic currents (Fig. 8*H*).

An additional factor is the role of the distribution of Na^+ channels. In this model, I_{Na} constitutes the major inward current and is located with the highest density in the axon and initial segment. To determine the influence of this distribution, simulations were performed with the use of uniform Na^+ channel density throughout the neuron. To generate overshooting spikes, this uniform density had to be increased to several times the estimate of Magee and Johnston (1995) in adult pyramidal cells (not shown), a conclusion also reached in other modeling studies (Mainen et al. 1995; Paré et al. 1997; Rapp et al. 1996). Simulations in which this nonrealistic uniform density was used had negligible influence on the properties of the bursts described above.

These features demonstrate that Cl^- bursts can be explained by a massive inward current in the somatic region, with little participation of dendritic currents. The perisomatic localization of the current underlying these bursts is also supported by morphological data. In cortical pyramidal cells, the largest density of GABAergic synapses is found in the somatic region, whereas excitatory synapses only appear in dendrites at >40 μm away from soma (reviewed in DeFelipe and Farinas 1992). Therefore in these cells the reversal of GABAergic IPSPs is likely to cause a strong inward current located mainly in the somatic region.

The model was then used to quantify the plausible range of GABAergic conductance densities leading to the observed bursts. With no EPSP present, GABAergic conductance densities that produced bursts, with morphology similar to that observed in experiments, were in the range of 0.6–6 mS/cm^2 in the proximal region. Adding dendritic EPSPs or IPSPs had only a small effect on the morphology of the burst (see Fig. 8). On the other hand, dendritic EPSPs and IPSPs significantly affected the EPSP/IPSP sequence in control conditions. The density of dendritic AMPA and NMDA conductance that gave rise to EPSPs of correct amplitude and phase in the soma was in the range of 5–7.5 mS/cm^2, much narrower than IPSPs. These simulations were performed with the use of the layer V morphology shown in Fig. 6, but the same range of conductance densities also applied to the layer VI cell (not shown).

The range of conductance values given above is only indicative, because the shape of the burst and the features of the EPSP/IPSP sequence in the soma varied depending on these values. For example, GABAergic conductance densities close to 6 mS/cm^2 gave rise to IPSPs of large amplitude in the soma and the Cl^- bursts led to spike inactivation, as sometimes seen during the experiments. The optimal set of conductance densities was ~6.3 mS/cm^2 for dendritic AMPA and NMDA, 1 mS/cm^2 for dendritic GABA, and 3 mS/cm^2 for GABA in soma and proximal dendrites. A ratio of ~1:3 between somatic and dendritic GABAergic conductance corresponds to the ratio of density of inhibitory synapses in soma and dendrites of cortical pyramidal cells (DeFelipe and Farinas 1992).

Finally, we investigated the spatial profile of V_m and Ca^{2+} following thalamic stimulation in the model. Although thalamic stimulation is subthreshold in the soma (Fig. 9*A*), there can be significant voltage transients in the dendrites (Fig. 9*B*). In the example of Fig. 9, there were Na^+ and Ca^{2+} spikes in the dendrites following simulated thalamic stimulation. However, the critical amount of proximal inhibition determined above drastically attenuated somatic invasion of these transients. Because of the activation of dendritic Ca^{2+} currents, the voltage transients were paralleled by significant Ca^{2+} entry in the dendrites (Fig. 9*C*). Thalamic-induced Ca^{2+} transients in cortical pyramidal cells were indeed recorded in vivo with the use of Ca^{2+} imaging techniques (Hirsch et al. 1995).

DISCUSSION

Intracellular recordings

The main finding of the present experimental work is that, during the sleep oscillatory state associated with spindles, spontaneous synchronized thalamic inputs to neocortex are

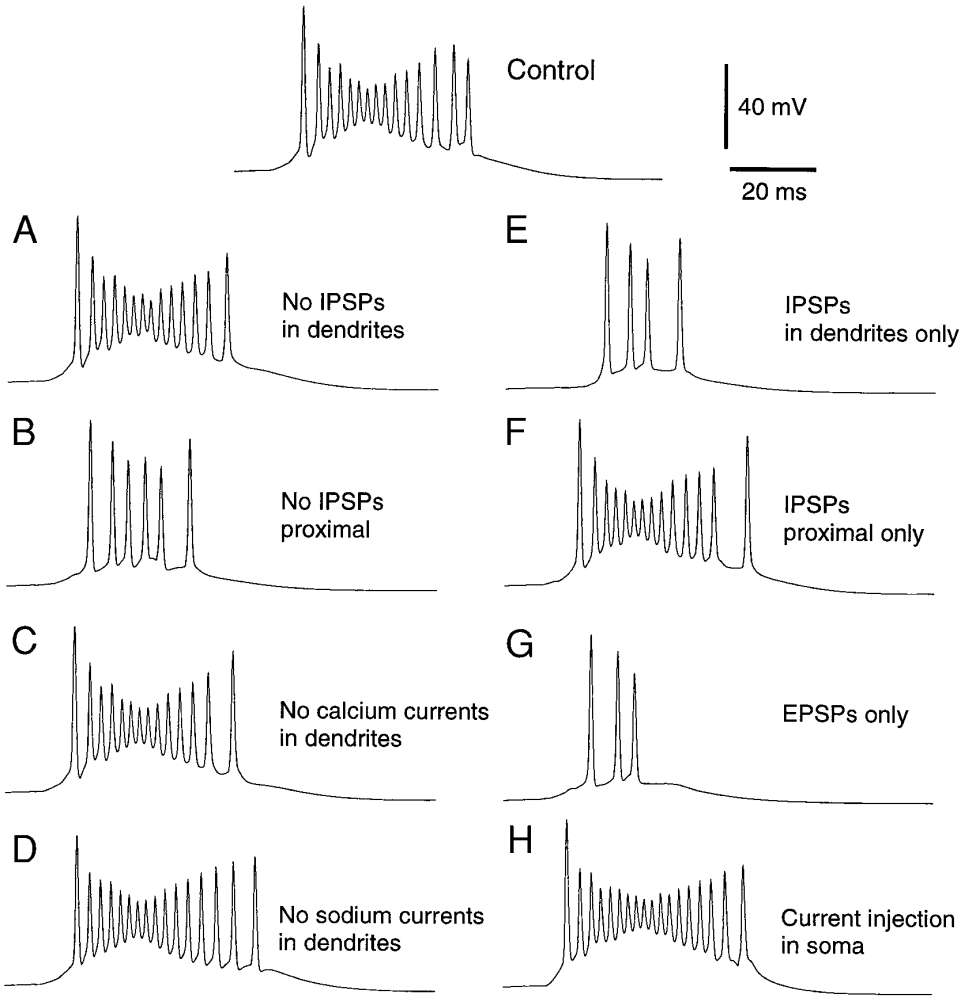

FIG. 8. Somatic and dendritic contributions to burst morphology. Same simulation as in Fig. 7*C*, *bottom* (0 mV reversal), was repeated by removing or adding currents in various regions of cell. *A*: removal of all GABAergic conductances in dendrites. *B*: removal of all GABAergic conductances in soma and most proximal part (40 μm) of dendrites. *C*: suppression of dendritic Ca^{2+} currents. *D*: removal of dendritic Na^{+} currents. *E*: dendritic IPSPs only (all EPSPs and proximal IPSPs removed). *F*: proximal IPSPs only (no EPSPs). *G*: EPSPs only (no IPSPs). *H*: burst following injection of a triangular ramp current in soma (ascending ramp from 0 to 10 nA in 22.5 ms followed by a descending ramp of same duration from 10 nA back to 0 nA).

heavily controlled by intracortical local inhibition. During spindles, TC cells fire spike bursts at the offset of GABAergic IPSPs (Steriade et al. 1993). The spindle-related IPSPs are imposed by thalamic reticular neurons because, after disconnection from thalamic reticular inputs, TC cells display much shorter and arrhythmic IPSPs (Steriade et al. 1985). Because of the divergence of connections from the thalamic reticular nucleus, and mainly from its rostral sector, to TC cells within various dorsal thalamic nuclei (Jones 1985; Steriade et al. 1984), IPSPs occur synchronized in populations of TC cells and consequently their postinhibitory rebound spike bursts are also synchronized. Quantitative analyses of thalamic burst patterns during natural sleep have shown that each burst of TC cells contains two to six spikes at frequencies >200 Hz (Domich et al. 1986), which represents a strong synaptic input to cortical cells. Because thalamic inputs to the cortex make excitatory synaptic contacts with local interneurons (Jones 1981, 1985; Toyama et al. 1974; White 1981), it is reasonable to assume that local inhibition plays an important role in controlling those inputs. However, no previous work had assessed this problem specifically. Blocking local cortical inhibition with $GABA_A$ receptor antagonists, such as bicuculline, is not an adequate approach for estimation of the degree of inhibition associated to TC synchronized inputs because, on extracellular application of $GABA_A$ antagonists, excitatory inputs of cortical origin are exceedingly enhanced because of the disinhibition of local populations and the high density of corticocortical connections, therefore blurring TC inputs.

We explored the presence of inhibition during synchronized thalamic inputs by injecting Cl^- ions intracellularly in neocortical cells from SI and suprasylvian association cortex (area 5), which are areas that clearly display spindle oscillations during barbiturate anesthesia and natural sleep (Andersen and Andersson 1968; Morison and Dempsey 1942; Steriade et al. 1990). As Cl^- ions leaked into the cell, the reversal potential of Cl^- shifted toward positive values and GABAergic IPSPs became depolarizing events. The amount by which the amplitude of spindle-related depolarizing events increased was, therefore, a direct measure of the amount of GABAergic inhibition that was activated by the incoming bursts of TC cells at each spindle wave. The change in sign of the IPSPs by Cl^- does not, however, prevent the increase in conductance that these synaptic events represent; therefore the recorded synaptic potentials are underestimations of the real amplitude of inhibitory inputs.

Two consequences derive from the present findings: *1*) the strength of thalamic input during sleep spindles is

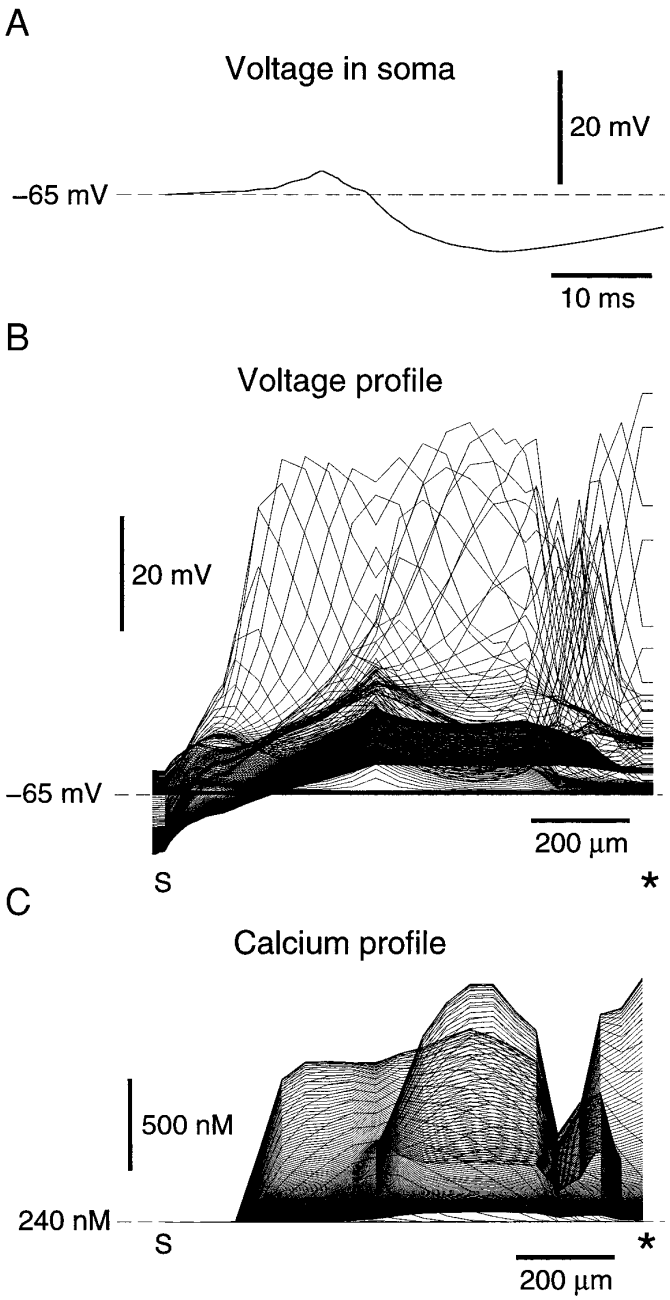

FIG. 9. Predicted dendritic voltage and Ca^{2+} transients during synchronized thalamic inputs. EPSP/IPSP sequence following simulated thalamic input is shown in soma and dendrites (same simulation as in Fig. 7*C*, *top*, with −80-mV reversal). *A*: EPSP/IPSP sequence in soma. *B*: profiles of voltage along a path from soma (S) to distal apical dendrite (*; indicated in Fig. 7*A*). Instantaneous profiles taken every 0.2 ms were superimposed. High-amplitude Na^+- and Ca^{2+}-dependent transients were seen in dendrites but not in soma. *C*: profiles of intracellular Ca^{2+} concentration represented as in *B*. Intracellular Ca^{2+} concentration was calculated in a thin shell (0.1 μm) beneath membrane.

stronger than it could have been predicted on the basis of the low firing rates of cortical cells during spindling; and *2*) blockage of inhibition at the cortical level may underlie the interictal spikes associated with spindling that are observable in the EEG (see INTRODUCTION). The first consequence has the important implication that in the dendrites of pyramidal cells, where synapses are mostly excitatory (DeFelipe and Fariñas 1992), there must be an important depolarization during sleep spindles that is not visible at the somatic level but that may activate Ca^{2+} currents leading to various phenomena of plasticity. The second consequence supports the hypothesis that an alteration of local cortical inhibition alone is enough to generate interictal spikes that appear interspersed within spindles after injections of bicuculline in the cortex (Contreras and Steriade, unpublished data).

Computational models

The main conclusion of the modeling study is that the transformation of EPSP/IPSP sequence to fully developed bursts in chloride-filled pipettes critically needs an important amount of inhibition in the cell. It was not possible to explain these results if the cell was dominated by EPSPs with weak IPSPs or with no IPSP at all. For different distributions of synaptic inputs and different values of conductances, the model consistently indicated that a relatively high density of inhibitory currents must be located in soma and proximal dendrites to account for the observed bursts.

A corollary observation is that the morphology of chloride bursts can be explained without the need of Ca^{2+} currents in the dendrites. Our model has dendritic Na^+ and Ca^{2+} currents, but removal of these currents did not dramatically influence the shape of the burst. The model therefore suggests that this type of burst essentially involves mechanisms located in the somatic region, with little dendritic participation. Further experiments would be needed to confirm this prediction. In particular, blocking Ca^{2+} currents or I_{Na} in the dendrites should have little influence on the shape of chloride bursts.

The relatively important amount of inhibition found in the model also suggests that in normal conditions, there is a relatively large amount of inhibitory cells recruited by ascending TC fibers. Therefore, during thalamic synchronized oscillations, we can expect the synaptic activation of the pyramidal cell to be dominated by inhibitory inputs. This would account for the observation that these cells have a relatively low level of discharge during spindling (Steriade and Deschênes 1984), although thalamic cells produce powerful bursts of action potentials.

The model provides a quantification of plausible distributions of synaptic inputs to soma and dendrites. The model directly predicts considerable voltage transients and Ca^{2+} entry in dendrites during synchronized thalamic inputs, with little influence on the soma. Such voltage and Ca^{2+} transients in dendrites, with well-controlled somatic spiking, may be ideal for triggering plasticity changes in pyramidal cells. Whether sleep-related synchronized thalamic bursting represents an input for plasticity in the cortex is an intriguing idea that still remains to be explored.

Experiments and models therefore point to the conclusion that, during synchronized thalamic input, cortical pyramidal cells receive strong excitation but are subject to a strict control by inhibitory interneurons. An important possible consequence of this observation is that a little change in the strength of inhibition may have drastic consequences at the network level. For example, a decrease in the strength of

fast, $GABA_A$-mediated inhibition will lead to enhanced firing of pyramidal cells, therefore providing more excitation to other pyramids, possibly leading to an avalanche of discharges and epileptic phenomena.

We thank G. Oakson, P. Giguère, and D. Drolet for technical assistance. We thank D. Amaral and T. J Sejnowski for the opportunity to use a neuron tracing system.

This work was supported by grants from the Medical Research Council of Canada, Human Frontier Science Program, and Fonds de la Recherche en Santé du Québec. D. Contreras was a Ph.D. student supported by the Savoy Foundation.

Address reprint requests to M. Steriade.

Received 15 November 1996; accepted in final form 20 March 1997.

REFERENCES

ANDERSEN, P. AND ANDERSSON, S. A. *Physiological Basis of the Alpha Rhythm.* New York: Appleton-Century-Crofts, 1968.

BLACK, J. A., KOCSIS, J. D., AND WAXMAN, S. G. Ion channel organization of the myelinated fiber. *Trends Neurosci.* 13: 48–54, 1990.

CHAGNAC-AMITAI, Y., LUHMANN, J., AND PRINCE, D. A. Burst generating and regular spiking layer 5 pyramidal neurons of rat neocortex have different morphological features. *J. Comp. Neurol.* 296: 598–613, 1990.

CONNORS, B. W., GUTNICK, M. J., AND PRINCE, D. A. Electrophysiological properties of neocortical neurons in vitro. *J. Neurophysiol.* 48: 1302–1320, 1982.

CONTRERAS, D., DESTEXHE, A., SEJNOWSKI, T. J., AND STERIADE, M. Control of spatiotemporal coherence of a thalamic oscillation by corticothalamic feedback. *Science Wash. DC* 274: 771–774, 1996.

CONTRERAS, D., DESTEXHE, A., SEJNOWSKI, T. J., AND STERIADE, M. Spatiotemporal patterns of spindle oscillations in cortex and thalamus. *J. Neurosci.* 17: 1179–1196, 1997.

CONTRERAS, D. AND STERIADE, M. Spindle oscillations in cats: the role of corticothalamic feedback in a thalamically generated rhythm. *J. Physiol. Lond.* 490: 159–179, 1996.

CREUTZFELDT, O. D., WATANABE, S., AND LUX, H. D. Relations between EEG phenomena and potentials of single cortical cells. II. Spontaneous and convulsoid activity. *Electroencephalogr. Clin. Neurophysiol.* 20: 19–37, 1966.

DEFELIPE, J. AND FARIÑAS, I. The pyramidal neuron of the cerebral cortex: morphological and chemical characteristics of the synaptic inputs. *Prog. Neurobiol.* 39: 563–607, 1992.

DESTEXHE, A., BABLOYANTZ, A., AND SEJNOWSKI, T. J. Ionic mechanisms for intrinsic slow oscillations in thalamic relay neurons. *Biophys. J.* 65: 1538–1552, 1993.

DESTEXHE, A., MAINEN, Z. F., AND SEJNOWSKI, T. J. An efficient method for computing synaptic conductances based on a kinetic model of receptor binding. *Neural Comput.* 6: 14–18, 1994.

DESTEXHE, A., MAINEN, Z. F., AND SEJNOWSKI, T. J. Kinetic models of synaptic transmission. In: *Methods in Neuronal Modeling* (2nd ed.), edited by C. Koch and I. Segev. Cambridge, MA: MIT Press. In press.

DOMICH, L., OAKSON, G., AND STERIADE, M. Thalamic burst patterns in the naturally sleeping cat: a comparison between cortically-projecting and reticularis neurones. *J. Physiol. Lond.* 379: 429–450, 1986.

EVARTS, E. V. Temporal patterns of discharge of pyramidal tract neurons during sleep and waking in the monkey. *J. Neurophysiol.* 27: 152–171, 1964.

FARIÑAS, I. AND DEFELIPE, J. Patterns of synaptic input on corticocortical and corticothalamic cells in the cat visual cortex. I. The cell body. *J. Comp. Neurol.* 304: 53–69, 1991a.

FARIÑAS, I. AND DEFELIPE, J. Patterns of synaptic input on corticocortical and corticothalamic cells in the cat visual cortex. II. The axon initial segment. *J. Comp. Neurol.* 304: 70–77, 1991b.

GLOOR, P., AVOLI, M., AND KOSTOPOULOS, G. Thalamocortical relationships in generalized epilepsy with bilaterally synchronous spike-and-wave discharge. In: *Generalized Epilepsy,* edited by M. Avoli, P. Gloor, G. Kostopoulos, and R. Naquet. Boston, MA: Birkhäuser, 1990, p. 190–212.

GLOOR, P., PELLEGRINI, A., AND KOSTOPOULOS, G. K. Effects of changes in cortical excitability upon the epileptic bursts in generalized penicillin epilepsy of the cat. *Electroencephalogr. Clin. Neurophysiol.* 46: 274–289, 1979.

GLOOR, P., QUESNEY, L. F., AND ZUMSTEIN, H. Pathophysiology of generalized penicillin epilepsy in the cat: the role of cortical and subcortical structures. *Electroencephalogr. Clin. Neurophysiol.* 43: 79–94, 1977.

GUTFREUND, Y., YAROM, Y., AND SEGEV, I. Subthreshold oscillations and resonant frequency in guinea-pig cortical neurons: physiology and modelling. *J. Physiol. Lond.* 483: 621–640, 1995.

HERKENHAM, M. Laminar organization of thalamic projections to the rat neocortex. *Science Wash. DC* 207: 532–535, 1980.

HESSLER, N., SHIRKE, A., AND MALINOW, R. The probability of transmitter release at a mammalian central synapse. *Nature Lond.* 366: 569–572, 1993.

HINES, M. NEURON: a program for simulation of nerve equations. In: *Neural Systems: Analysis and Modeling,* edited by F. Eekman. Boston, MA: Kluwer, 1993, p. 127–136.

HIRSCH, J. A., ALONSO, J. M., AND REID, C. L. Visually evoked calcium action potentials in cat striate cortex. *Nature Lond.* 378: 612–616, 1995.

HODGKIN, A. L. AND HUXLEY, A. F. A quantitative description of membrane current and its application to conduction and excitation in nerve. *J. Physiol. Lond.* 117: 500–544, 1952.

HUGUENARD, J. R., HAMILL, O. P., AND PRINCE, D. A. Sodium channels in dendrites of rat cortical pyramidal neurons. *Proc. Natl. Acad. Sci. USA* 86: 2473–2477, 1989.

JASPER, H. AND STEFANIS, C. Intracellular oscillatory rhythms in pyramidal tract neurones in the cat. *Electroencephalogr. Clin. Neurophysiol.* 18: 541–553, 1965.

JONES, E. G. Anatomy of cerebral cortex: columnar input-output organization. In: *The Organization of the Cerebral Cortex,* edited by F. O. Schmitt, F. G. Worden, G. Adelman, and S. G. Dennis. Cambridge, MA: MIT Press, 1981, p. 199–234.

JONES, E. G. *The Thalamus.* New York: Plenum, 1985.

JONES, E. G. AND POWELL, T. Morphological variations in the dendritic spines of the neocortex. *J. Cell Sci.* 5: 509–529, 1969.

JONES, E. G. AND POWELL, T. Electron microscopy of the somatic sensory cortex of the cat. I. Cell types and synaptic organization. *Philos. Trans. R. Soc. Lond. B Biol. Sci.* 257: 1–11, 1970.

LANG, E. AND PARÉ, D. Synaptic and synaptically-activated intrinsic conductances underlie inhibitory potentials in cat lateral amygdaloid projection neurons in vivo. *J. Neurophysiol.* 77: 353–363, 1997.

LARKMAN, A. U. Dendritic morphology of pyramidal neurones of the visual cortex of the rat: III. Spine distributions. *J. Comp. Neurol.* 306: 332–343, 1991.

MAGEE, J. AND JOHNSTON, D. Synaptic activation of voltage-gated channels in the dendrites of hippocampal pyramidal neurons. *Science Wash. DC* 268: 301–304, 1995.

MAINEN, Z. F., JOERGES, J., HUGUENARD, J. R., AND SEJNOWSKI, T. A model of spike initiation in neocortical pyramidal neurons. *Neuron* 15: 1427–1439, 1995.

MATSUMOTO, H. AND AJMONE-MARSAN, C. Cortical cellular phenomena in experimental epilepsy: interictal manifestations. *Exp. Neurol.* 9: 286–304, 1964.

MCCORMICK, D. A., CONNORS, B. W., LIGHTHALL, J. W., AND PRINCE, D. A. Comparative electrophysiology of pyramidal and sparsely spiny stellate neurons of the neocortex. *J. Neurophysiol.* 54: 782–806, 1985.

MORISON, R. S. AND DEMPSEY, E. W. A study of thalamocortical relations. *Am. J. Physiol.* 135: 281–292, 1942.

MUNGAI, J. M. Dendritic patterns in the somatic sensory cortex of the cat. *J. Anat.* 101: 403–418, 1967.

NUÑEZ, A., AMZICA, F., AND STERIADE, M. Electrophysiology of cat association cortical cells in vivo: intrinsic properties and synaptic responses. *J. Neurophysiol.* 70: 418–429, 1993.

OTIS, T. S. AND MODY, I. Modulation of decay kinetics and frequency of $GABA_A$ receptor-mediated spontaneous inhibitory postsynaptic currents in hippocampal neurons. *Neuroscience* 49: 13–32, 1992.

PARÉ, D., LANG, E. J., AND DESTEXHE, A. Inhibitory control of somatic and dendritic sodium spikes in neocortical pyramidal neurons in vivo: an intracellular and computational study. *Neuroscience.* In press.

PETERS, A. AND KAISERMAN-ABRAMOF, I. R. The small pyramidal neuron of the rat cerebral cortex. The perikaryon, dendrites and spines. *Am. J. Anat.* 127: 321–356, 1970.

PETERS, A., SETHARES, C., AND HARRIMAN, K. M. Different kinds of axon terminals forming symmetric synapses with the cell bodies and initial

axon segments of layer II/III pyramidal cells. II. Synaptic junctions. *J. Neurocytol.* 19: 584–600, 1990.

PRESS, W. H., FLANNERY, B. P., TEUKOLSKY, S. A., AND VETTERLING, W. T. *Numerical Recipes. The Art of Scientific Computing.* Cambridge, UK: Cambridge Univ. Press, 1986.

PRINCE, D. A. AND CONNORS, B. W. Mechanisms of interictal epileptogenesis. In: *Advances in Neurology*, edited by A. V. Delgado-Escueta, A. A. Ward, D. M. Woodburry, and R. Porter. New York: Raven, 1986, p. 275–299.

PRINCE, D. A. AND FARRELL, D. ''Centrencephalic'' spike-wave discharges following parenteral penicillin injection in the cat. *Neurology* 19: 309–310, 1963.

RAPP, M., YAROM, Y., AND SEGEV, I. Modeling back propagating action potential in weakly excitable dendrites of neocortical pyramidal cells. *Proc. Natl. Acad. Sci. USA* 93: 11985–11990, 1996.

REUVENI, I., FRIEDMAN, A., AMITAI, Y., AND GUTNICK, M. J. Stepwise repolarization from Ca^{2+} plateaus in neocortical pyramidal cells: evidence for nonhomogeneous distribution of HVA Ca^{2+} channels in dendrites. *J. Neurosci.* 13: 4609–4621, 1993.

SAH, P. AND BEKKERS, J. M. Apical dendritic location of slow afterhyperpolarization current in hippocampal pyramidal neurons: implications for the integration of long-term potentiation. *J. Neurosci.* 16: 4537–4542, 1996.

STERIADE, M. Interneuronal epileptic discharges related to spike-and-wave cortical seizures in behaving monkeys. *Electroencephalogr. Clin. Neurophysiol.* 37: 247–263, 1974.

STERIADE, M. AND AMZICA, F. Dynamic synaptic coupling among cortical neurons during evoked and spontaneous spike-wave seizure activity. *J. Neurophysiol.* 72: 2051–2069, 1994.

STERIADE, M., AMZICA, F., AND NECKELMANN, D. Intracellular patterns of neocortical seizures including spike-wave (SW) and polyspike-wave (PSW) complexes at 2–4 Hz, in vivo. *Soc. Neurosci. Abstr.* In press.

STERIADE, M. AND CONTRERAS, D. Relations between cortical and thalamic cellular events during transition from sleep patterns to paroxysmal activity. *J. Neurosci.* 15: 623–642, 1995.

STERIADE, M. AND DESCHÊNES, M. The thalamus as a neuronal oscillator. *Brain Res. Rev.* 8: 1–63, 1984.

STERIADE, M., DESCHÊNES, M., DOMICH, L., AND MULLE, C. Abolition of spindle oscillations in thalamic neurons disconnected from nucleus reticularis thalami. *J. Neurophysiol.* 54: 1473–1497, 1985.

STERIADE, M., DESCHÊNES, M., AND OAKSON, G. Inhibitory processes and interneuronal apparatus in motor cortex during sleep and waking. I. Background firing and responsiveness of pyramidal tract neurons and interneurons. *J. Neurophysiol.* 37: 1065–1092, 1974.

STERIADE, M., JONES, E. G., AND LLINÁS, R. R. *Thalamic Oscillations and Signaling.* New York: Wiley-Interscience, 1990.

STERIADE, M., MCCORMICK, D. A., AND SEJNOWSKI, T. J. Thalamocortical oscillations in the sleeping and aroused brain. *Science Wash. DC* 262: 679–685, 1993.

STERIADE, M., PARENT, A., AND HADA, J. Thalamic projections of nucleus reticularis thalami: a study using retrograde transport of horseradish peroxidase and double fluorescent tracers. *J. Comp. Neurol.* 229: 531–547, 1984.

STUART, G. J. AND SAKMANN, B. Active propagation of somatic action potentials into neocortical pyramidal cell dendrites. *Nature Lond.* 367: 69–72, 1994.

TOYAMA, T., MATSUNAMI, K., OHNO, T., AND TOKASHIKI, S. An intracellular study of neuronal organization in the visual cortex. *Brain Res.* 14: 518–520, 1974.

TRAUB, R. D. AND MILES, R. *Neuronal Networks of the Hippocampus.* Cambridge, UK: Cambridge Univ. Press, 1991.

WHITE, E. L. Thalamocortical synaptic relations. In: *The Organization of the Cerebral Cortex*, edited by F. O. Schmitt, F. G. Worden, G. Adelman, and S. G. Dennis. Cambridge, MA: MIT Press, 1981, p. 153–161.

WHITE, E. L. *Cortical Circuits.* Boston, MA: Birkhäuser, 1989.

XIANG, Z., GREENWOOD, A. C., AND BROWN, T. Measurement and analysis of hippocampal mossy-fiber synapses. *Soc. Neurosci. Abstr.* 18: 1350, 1992.

YUSTE, R. AND TANK, D. W. Dendritic integration in mammalian neurons, a century after Cajal. *Neuron* 16: 701–716, 1996.